Revisiting scoliosis in the KNM-WT 15000 Homo erectus skeleton

Schiess, Regula ; Böni, Thomas ; Rühli, Frank J ; Häusler, Martin

DOI: https://doi.org/10.1016/j.jhevol.2013.12.009

Revisiting scoliosis in the KNM-WT 15000 *Homo erectus* skeleton

Regula Schiess[a] & Thomas Boeni[b,c] Frank Rühli [c] & Martin Haeusler[a,b,c,1]

[a] *Anthropological Institute and Museum, University of Zuerich, Winterthurerstrasse 190, 8057 Zuerich, Switzerland*

[b] *Orthopaedische Universitaetsklinik Balgrist, Forchstrasse 340, 8008 Zuerich, Switzerland*

[c] *Centre for Evolutionary Medicine, Institute of Anatomy, University of Zuerich, Winterthurerstrasse 190, 8057 Zuerich, Switzerland*

[1] Corresponding author:

Centre for Evolutionary Medicine, Institute of Anatomy, University of Zuerich,

Winterthurerstrasse 190, 8057 Zuerich, Switzerland

MartinFelix.Haeusler@uzh.ch

Tel. +41 44 635 55 26, Cell + 41 77 448 57 86

Keywords:

Early hominins, vertebral column, human evolution, palaeopathology, adolescent idiopathic scoliosis

Abstract

Owing to its completeness, the 1.5 million year old Nariokotome boy skeleton KNM-WT 15000 is central for understanding skeletal biology of *Homo erectus*. Nevertheless, since Latimer and Ohman (2001, Axial dysplasia in *Homo erectus*. J Hum Evol 40:A12) reported on asymmetries and distortions of Nariokotome boy's axial skeleton suggesting adolescent idiopathic scoliosis, possibly associated with congenital skeletal dysplasia, it is questionable whether it still can be used as reference for *Homo erectus*. Recently, however, the presence of skeletal dysplasia has been refuted. Here, we present a morphologic and morphometric reanalysis of the assertion of idiopathic scoliosis. We demonstrate that unarticulated vertebral columns of non-scoliotic and scoliotic individuals can be distinguished based on the lateral deviation of the spinous process, lateral and sagittal wedging, vertebral body torsion, pedicle thickness asymmetry and asymmetry of the superior and inferior articular facet area. A principal component analysis of the overall asymmetry of all seven vertebral shape variables groups KNM-WT 15000 within non-scoliotic modern humans. An anomaly of vertebrae T1-T2 is compatible with a short left convex curve at the uppermost thoracic region, possibly due to injury or local growth dysbalance. Asymmetries of the facet joints L3-L5 suggest a local right convex curve in the lower lumbar region that probably resulted from juvenile traumatic disc herniation. This pattern is incompatible with adolescent idiopathic scoliosis or other types of scoliosis, including congenital, neuromuscular or syndromic scoliosis. It is, however, consistent with a recent reanalysis of the rib cage that did not reveal any asymmetry. Except for these possibly trauma-related anomalies, the Nariokotome boy fossil therefore seems to belong to a normal *Homo erectus* youth without evidence for adolescent idiopathic scoliosis or other severe pathologies of the axial skeleton.

Introduction

The 1.53 million year old KNM-WT 15000 skeleton of a *Homo erectus* boy from Nariokotome, West Lake Turkana, Kenya, is a key fossil for studying early *Homo* biology and behaviour (Walker and Leakey, 1993a). However, since Latimer and Ohman (2001) and Ohman et al. (2002) described serious deformities of his axial skeleton the validity of inferences from this important specimen is questioned. Based on a number of asserted pathologies including diminutive and platyspondylic vertebrae, spina bifida, condylus tertius, spinal stenosis, and scoliosis with associated vertebral, rib and clavicular distortions, these authors suggested the presence of congenital skeletal dysplasia leading to disproportionate dwarfism. A recent reanalysis of this symptom complex demonstrated, however, that the KNM-WT 15000 vertebrae are not flat relative to their cross-sectional area if compared to modern humans of the same skeletal age (Schiess and Haeusler, 2013). The vertebrae are therefore not platyspondylic, thus refuting the presence of disproportionate dwarfism and skeletal dysplasia. Furthermore, there is no evidence for spina bifida *sensu stricto* in KNM-WT 15000, and the condylus tertius is not related to skeletal dysplasias (Schiess and Haeusler, 2013). On the other hand, the relatively small size of the vertebrae and the narrow spinal canal in the cervical region probably are characteristics of early hominins in general rather than congenital pathologies (Robinson, 1972; Day and Leakey, 1974; McHenry, 1992; MacLarnon and Hewitt, 2004; Lordkipanidze et al., 2007; Schiess and Haeusler, 2013).

So far, however, Latimer and Ohman's (2001) assertion of scoliosis and associated skeletal asymmetries in KNM-WT 15000 has not been evaluated in detail. There is only one review that affirmed the diagnosis of adolescent idiopathic scoliosis based on the observation of "both thoracic asymmetry and vertebral fracture" (Lovejoy, 2005: 103). Yet vertebral fracture is not known to lead to idiopathic scoliosis (Weinstein et al., 2008), and a recent analysis of the KNM-WT 15000 axial skeleton found no evidence for fractured vertebrae

(Haeusler et al., 2011). Moreover, no substantial asymmetry of the rib cage remains after a re-alignment of the ribs (Haeusler et al., 2011). This challenges a significant scoliotic curve in the thoracic region. Instead, anterior curved remodelling of the superior facet joint of L5 and formation of a nearthorsis indicate facet joint subluxation of the last two lumbar vertebrae. Haeusler et al. (2013) thus concluded that KNM-WT 15000 suffered from disc herniation L4–5.

Nevertheless, a visual inspection of the KNM-WT 15000 skeleton reveals a marked lateral deviation of upper thoracic spinous processes and asymmetrical facet joints in the lower lumbar region. The aim of the present study is therefore a reanalysis of these vertebral asymmetries using a three-dimensional morphometric approach. Thus, we will evaluate whether the asymmetries can be caused by idiopathic scoliosis and we will propose a differential diagnosis.

Adolescent idiopathic scoliosis

Scoliosis is a complex three-dimensional deformity of the axial skeleton. It is characterized by a lateral spinal curve in the coronal plane that must be greater than 10° (measured according to Cobb, 1948) coupled with an abnormal curvature in the sagittal plane and a rotational deformation in the transversal plane (Stokes, 1994; Perdriolle et al., 2001). Untreated, it can lead to curve progression, back pain, and psychosocial restrictions. Eventually, particularly in early-onset forms, cardiopulmonary problems are feared, although the severity of these conditions and their effects on overall health is very variable (Asher and Burton, 2006; Weinstein et al., 2008).

Based on its aetiology, different types of scoliosis have been recognized, including idiopathic scoliosis and the far less common neuromuscular, syndromic and congenital forms (Goldstein and Waugh, 1973). Congenital scoliosis is defined as resulting from failure of

formation or failure of segmentation like hemi-vertebrae and block vertebrae, respectively, while syndromic scoliosis is associated with a genetic syndrome, and neuromuscular scoliosis with neuropathic and myopathic diseases (Hedequist and Emans, 2007; Vialle et al., 2013). The diagnosis of idiopathic scoliosis can only be made after these other forms of scoliosis have been excluded (Goldstein and Waugh, 1973). According to the three peak periods of onset – under the age of three, from five to eight, and from ten until the end of growth, idiopathic scoliosis is classified as infantile, juvenile and adolescent (James, 1954). The most frequent, and least severe, type is adolescent idiopathic scoliosis that accounts for 85% of cases of scoliosis. It affects about 2.5% of the modern population, of whom up to 10% need active treatment (Kane, 1977; Miller, 1999).

Adolescent idiopathic scoliosis not only is the most frequent type of scoliosis in modern humans, the deformity is also restricted to the species *Homo*. All forms of scoliosis described in other vertebrates are either congenital, neuromuscular, cicatricial or experimentally induced (Kouwenhoven and Castelein, 2008). The possible presence of adolescent idiopathic scoliosis in KNM-WT 15000 would therefore constitute the earliest case of this deformity, thus suggesting upright bipedalism as a prerequisite for its development.

Material and Methods

Samples

The Nariokotome *Homo erectus* boy skeleton KNM-WT 15000 is the most complete early hominin yet found (Brown et al., 1985; Walker and Leakey, 1993a). The axial skeleton preserves the last cervical vertebrae, ten thoracic vertebrae and twelve pairs of ribs, all five lumbar vertebrae, and five sacral elements. Our identification of the vertebrae is according to Haeusler et al. (2011; see also Haeusler et al., 2002; Haeusler et al., 2012; Williams, 2012). Consequently, we base our analysis on the presence of 5 lumbar and 12 thoracic vertebrae,

which it is modal in modern humans, rather than on 6 lumbar elements, as described by Walker and Leakey (1993b).

Our comparative sample included 23 normal modern human vertebral columns without macroscopic anomalies (4 young adult individuals and 19 subadults with dental ages between 9 and 18 years), and 10 scoliotic spines (2 subadults with dental ages of 11 and 13 years and 8 young adult individuals, i.e., with not completely fused vertebral ring apophyses and without degenerative alterations). Although the skeletal age of KNM-WT 15000 is comparable to 12 to 15 years old modern humans (Ruff and Walker, 1993; Smith, 1993; Tardieu, 1998), it seems unlikely that the inclusion of young adult specimens into our reference sample had an effect on our analyses of vertebral torsion and asymmetry. Adolescent idiopathic scoliosis most rapidly progresses during the pubertal growth spurt, but only slowly if at all after skeletal maturity (Weinstein et al., 1981; Dimeglio et al., 2011). Four spinal curves of our sample can qualitatively be described as "slightly scoliotic", and six, including the two subadult specimens, as "markedly scoliotic". Apart from three articulated scoliotic specimens from pathological collections of the early 20th century, all skeletons stem from archaeological excavations in Switzerland. They are housed in the Anthropological Institute and Museum of the University of Zuerich, the Centre of Evolutionary Medicine, Institute of Anatomy, University of Zuerich, the Historical Anthropology of the University of Bern, the Natural History Museum Basel, and the Anthropological Research Institute Aesch.

Scoliosis

The standard definition of scoliosis is a lateral deviation of the spine with a Cobb angle greater than 10° on a postero-anterior standing radiograph, deviations between 0° and 10° being regarded as negligible (Kane, 1977). This definition is not operative in a bio-archaeological and palaeoanthropological context, where only a gross qualitative assessment

of the lateral curve is possible in articulated, supine interred skeletons. Yet, the deformity also affects the individual vertebrae and associated structures, leading to the characteristic rib hump on the convex side of the thoracic curve and a deviation of the spinous processes to the concave side (Fig. 1). Morphometric studies further demonstrated a decreased pedicular width on the concavity of the curve, increased lateral wedging of the vertebral bodies towards the apex of the curve, and facet surface asymmetries (Liljenqvist et al., 2000; Parent et al., 2002; Parent et al., 2004b).

Data acquisition

In accordance to the variables analyzed by Liljenqvist et al. (2000) and Parent et al. (2002; 2004b), 35 3D-landmarks per vertebra were recorded by one of us (R.S.) using a MicroScribe G2 (Immersion Corporation, San José, CA, USA; Fig. 2). Digitizing of the KNM-WT 15000 vertebrae was done on casts, but distances between the landmarks have been checked for accuracy against the originals. Based on the landmark coordinates, seven shape variables per vertebra have been calculated (Table 1).

Measurement error

The MicroScribe G2 has a reported accuracy of ± 0.38 mm. Several additional observer-induced sources of error unique to the acquisition of 3D coordinates contribute to the total landmark error (von Cramon-Taubadel et al., 2007). One source of error stems from the difficulty of a direct visual control of the landmark position during the digitization process. Moreover, not all landmarks are equally identifiable, which lead Bookstein (1991) to distinguish three types of landmarks. Type I landmarks are defined by compositional evidence such as the intersection of sutures, Type II landmarks are at geometric maxima of bony

protrusions or depressions and Type III landmarks are at extreme locations with respect to other landmarks or geometric entities.

To evaluate the intra-observer error in recording the landmarks, a mid-thoracic and a mid-lumbar modern human vertebra were digitized five times by R.S. Repeats from the same specimens were superimposed using Generalized Procrustes Analysis with Morphologika 2.5 (O'Higgins and Jones, 2006) without scaling the landmark sets. The Pinocchio effect inherent to Procrustes superimposition (von Cramon-Taubadel et al., 2007) is deemed negligible due to the relatively large number of 35 landmarks. Based on the five trials we calculated the centroid for each landmark. The measurement error of the landmark is then represented by the median of the Euclidian distances of the individual landmark repeats from the centroid (Table 2). It ranged between 0.2 mm for landmark 23 (supero-lateral extremity of right superior articular facet, Type II) and 1.6 mm for landmark 6 (lateral basis of right pedicle, Type III), with an overall error of measurement of 0.5 mm. The magnitude of the overall measurement error is identical to that reported in a morphometric study of scoliotic spines using a Fastrack coordinate measuring machine (Parent et al., 2002) and very similar to MicroScribe-based studies of cranial landmarks (0.1 mm to 1.4 mm, von Cramon-Taubadel et al., 2007; 0.3 mm to 1.57 mm, Sholts et al., 2011).

The error of measurement (TEM) provides an estimate of the typical magnitude of measurement error of the seven shape variables calculated from the 3D landmarks. The TEM is in the units of measurement and is computed as follows:

$$TEM = \sqrt{\frac{\sum_{i=1}^{N}\left[\sum_{j=1}^{K} x_j^2 - \frac{\left(\sum_{j=1}^{K} x_j\right)^2}{K}\right]}{N(K-1)}}$$

where x is the measurement of the j^{th} replicate (j=1, 2, …, K), K the number of replicates, and N the number of subjects, in this case N = 1 (Dahlberg, 1940; Mueller and Martorell, 1988; Knapp, 1992). The TEM ranged between 0.02 and 0.11 for ratios and between 0.6° and 4.6° for angular measurements (Table 3). As the landmark error is independent of the size of the vertebra, the TEM was generally lower in the mid-lumbar vertebra than in the smaller mid-thoracic vertebra.

Principal component analysis

A principal component analysis (PCA) was used as a data reduction technique to explore the patterns from these variables with respect to non-scoliotic and scoliotic vertebral columns and KNM-WT 15000. In analogy to the standard deviations for these variables across the thoracolumbar vertebrae of a specimen, the principal component analysis was based on the roots of the means of the squared deviations from perfect symmetry (root mean square, RMS).

Results

Macroscopic inspection of KNM-WT 15000

Macroscopically, the spinous process of the first thoracic vertebra of KNM-WT 150000 (T1) clearly deviates to the left (Fig 3). Its tip and the tip of the T2 spinous process are, however, inflected to the right. The ends of the spinous processes of T1, T2 and L4 are also 10° - 20° twisted with respect to the sagittal plane and run from left cranially to right caudally (Fig. 4). In the lumbar region, the facet joints between L3/L4, L4/L5 and L5/S1 have noticeably asymmetric areas, lengths and shapes, which cannot be attributed to post-mortem

damage. Most remarkable is the large left superior facet joint of L5. Its tip is bent anteriorly and articulates with a nearthrosis at the inferior side of the left pedicle of L4.

The other vertebrae are macroscopically inconspicuous. We found no formation or segmentation defects like hemi-vertebrae and block vertebrae. Although the left costal process of L5 is slightly thicker compared to the right side, it is not bent caudally (Fig. 3 and Fig. 4). Hence, there is no evidence for asymmetric sacralisation that could also have caused scoliosis. Nevertheless, the tip of the left costal process of L5 is remarkable for its missing apophysis, which in modern humans usually forms at age 11 to 14 and later fuses to the costal process (Schmorl and Junghans, 1968). The apophysis of the tip of the right costal process seems to be already fused.

Morphometric analysis

A morphometric analysis of the KNM-WT 15000 thoracolumbar vertebral column compared to 23 normal and 10 scoliotic modern humans is presented in Table 4 and Fig. 5. This analysis demonstrated that the median of our normal, non-scoliotic sample does often not conform to perfect bilateral symmetry. Thus, the spinous processes of the lower thoracic vertebrae T10 to T12 on average significantly deviated up to 6.6° to the right with respect to the sagittal plane through the vertebral body; the vertebral bodies of T7 to T12 and L2 to L3 were distorted to the left; the vertebral bodies of T1, T10, L1, L4 and L5 were wedged to the left, and those of T4 and T7 were wedged to the right; the inferior articular facet joints of T2, T3 and T10 were larger on the right side, whereas those of L4 and L5 were larger on the left side; and the pedicle roots of T4 were thicker on the right side. In addition, the vertebral bodies of T1, T2, and T4 to L1 were kyphotically wedged, while they were lordotically wedged at L4 and L5.

These asymmetries were significantly more marked in scoliotic spines. Particularly near the apex of the curves, the 3rd-97th inter-percentile range of normal spines was substantially surpassed. The vertebral bodies typically were distorted towards the convex side of the curve, which was best visible at the thoracolumbar border. Also the spinous processes were pointed to the convex side, and pedicular width and facet joint areas were considerably smaller on the convex side (see also Fig 1). In addition, the majority of the scoliotic spines had an abnormal sagittal curvature with lordotic wedging in the thoracic region.

The shape of the KNM-WT 15000 vertebrae variously deviated from the median of our normal modern human sample, and some measurements exceeded the 3rd-97th inter-percentile range of normal spines. In the upper thoracic region, these included the lateral deviation of the spinous process of vertebra T1 and the asymmetries of the inferior articular facets of T1 and of the pedicle roots of T2. The angulation of the T1 spinous process of KNM-WT 15000 to the left suggests a left convex curve in the upper thoracic region. This is consistent both with the dimensions of the pedicles of T1 and T2 and the inferior facet joints of T1. All these measurements were slightly smaller on the left side than on the right side. At odds with a typical left convex scoliotic curve in the upper thoracic region were, however, the tips of the T1 and T2 spinous processes. They were bent to the right rather than to the convex left side as usually in scoliotic spines (see, e.g., Wever et al., 1999). The spinous processes of the adjacent vertebrae C7 and T3 did not deviate from the mid-sagittal plane (see also Fig 3), which implied an extraordinarily short scoliotic curve involving just T1 and T2. On the other hand, while still being within the 3rd-97th inter-percentile range of normal spines, the direction of the asymmetry of the inferior facet joints of T2 and T3, the superior facet joints of T1 to T3, and lateral wedging of T2 and T3 all suggested a discretely right convex curve.

In the mid-thoracic region of KNM-WT 15000, only the right pedicle of T7 was measured significantly larger than on the left side. Other measurements in this region were

within the range of normal variation. This includes a small deviation of the spinous process of T6 to the left and a discrete torsion of the vertebral bodies of T6 and T7 to the left side. Further, the inferior articular processes of T6 and T7 were slightly smaller on the left compared to the right side. All these characteristics, as well as lateral wedging at T4 and T6, but not at T7, could be compatible with a faint left convex curve in the mid-thoracic region.

At the thoracolumbar transition of KNM-WT 15000, the angulation of the spinous process to the sagittal plane, vertebral body torsion, lateral wedging, and the asymmetry of superior and inferior articular facet joint areas and pedicle thickness were all close to the median of normal spines. Only the lateral wedging of L1 was slightly right convex, though within the range of variation of non-scoliotic individuals.

In the lumbar spine of KNM-WT 15000, the asymmetry of the superior articular facets of L5 exceeded the 3^{rd}-97^{th} inter-percentile range of non-scoliotic spines. As the facet joint was measured larger on the left than on the right side, this suggested a right convex curve at the lower lumbar spine. Consistent with a right convex curve, though within the range of normal variation, was also the asymmetry of the inferior facet joint areas of L3, while the spinous processes of L3 and L4 indicated a curve to the opposite direction.

The overall picture that emerged despite some inconsistencies was a left convex curve in the coronal plane in the uppermost thoracic region and a right convex curve in the lower lumbar spine. In between, there was a possible discrete right convex curve at T3 and a left convex counter curve in the mid-thoracic region, although the asymmetries were here within the normal range of variation.

In the sagittal plane, our data did not indicate an abnormal sagittal spinal curvature (abnormal kyphosis or lordosis) in KNM-WT 15000. His vertebrae therefore contrasted with modern human spines with idiopathic scoliosis that usually displayed a hypokyphotic or even lordotic sagittal wedging in the thoracic region. Rather, the lower lumbar vertebrae were

slightly more lordotically wedged than on average in normal modern humans, while the vertebrae at the thoracolumbar junction were discretely more kyphotic. This is compatible with a sagittal spinal curvature of the Nariokotome boy at least as marked as on average in modern humans.

Principal component analysis

A principal component analysis (PCA) was run to reduce the number of vertebral shape variables into a smaller set of new variables. The PCA was based on the roots of the means of the squared deviations from perfect symmetry. Two principal components were extracted with eigenvalues greater than 1 that accounted for 65.1% of the explained variance (Table 5). Lateral and sagittal wedging, pedicle root asymmetry and vertebral body torsion primarily loaded on the first component (PC1), whereas variation in superior and inferior facet area asymmetry was mainly represented by PC2. The first principal component separated our sample of non-scoliotic and scoliotic modern human vertebral columns, although there was some overlap between a few non-scoliotic specimens and slightly scoliotic spines (Fig. 6). This overlap is expected since the transition from a physiologic spinal curvature to a scoliotic deformity is continuous. KNM-WT 15000 grouped close to the centroid of non-scoliotic spines, suggesting that the overall asymmetries of his vertebrae cannot be distinguished from normal variation. The same picture resulted when the PCA was run without the scoliotic individuals.

Discussion

Latimer and Ohman (2001) noted various abnormalities in the axial skeleton of the Nariokotome boy that they attributed both to skeletal dysplasia and idiopathic scoliosis. While a recent study found no support for the diagnosis of skeletal dysplasia (Schiess and Haeusler,

2013), the present work analyses the evidence for idiopathic scoliosis in KNM-WT 15000. This disorder is unknown in non-human vertebrates, yet it is the most common spinal deformity in modern humans (Kouwenhoven and Castelein, 2008). Because *Homo erectus* is the earliest human ancestor with a truly modern body shape and bipedal locomotion (Bramble and Lieberman, 2004; Haeusler and McHenry, 2004, 2007), it would not be totally unexpected if KNM-WT 15000 already suffered from adolescent idiopathic scoliosis.

Modern human boys affected by adolescent idiopathic scoliosis typically present at age 12 to 15 years, which is slightly later than in girls (Raggio, 2006). This seems to be at odds with the mean age estimate of 11 - 12 years for the Nariokotome boy (Smith, 1993). A still greater discrepancy is with his chronological age at death of approximately eight years that is implied by tooth microanatomy and tooth eruption (Dean et al., 2001; Smith, 2004; Zihlman et al., 2004). These age estimates better fit with juvenile rather than with adolescent idiopathic scoliosis. Juvenile idiopathic scoliosis has a peak age-at-onset of five to eight years (James, 1954). It is relatively uncommon compared to the adolescent-onset form of idiopathic scoliosis, and the deformity is generally more severe (Ponseti and Friedman, 1950; Figueiredo and James, 1981; Robinson and McMaster, 1996). However, *Homo erectus* seems to have matured faster than modern humans, as the pattern of epiphyseal union of KNM-WT 15000 matches that of 12 to 15-year-old modern humans (Ruff and Walker, 1993; Smith, 1993; Tardieu, 1998). His skeletal age is therefore well compatible with the potential presence of adolescent idiopathic scoliosis.

Another prerequisite for the progression of adolescent idiopathic scoliosis is the presence of an adolescent growth spurt (Lowe et al., 2000; Cheung et al., 2008), but it is disputed whether *Homo erectus* already evolved this distinctive human growth pattern (Smith, 1993; Tardieu, 1998; Smith, 2004; Zihlman et al., 2004; Graves et al., 2010).

Idiopathic scoliosis is a diagnosis by exclusion (Goldstein and Waugh, 1973). Its differential diagnosis mainly includes neuromuscular scoliosis, syndromic scoliosis and congenital scoliosis. In fact, a recent study found no indications that KNM-WT 15000 was affected by a neuromuscular disease or a genetic syndrome such as skeletal dysplasia (Schiess et al., 2006; Schiess and Haeusler, 2013). Congenital scoliosis can also be excluded due to the absence of bloc vertebrae, hemi-vertebrae or other segmentation and formation defects. Adolescent idiopathic scoliosis would therefore be the most likely form of scoliosis in the Nariokotome boy.

Because the clinical definition of scoliosis as a lateral curve with a Cobb angle > 10° is not applicable to a palaeoanthropological context, the present study uses a morphometric approach similar to that of Liljenqvist et al. (2000) and Parent et al (2002; 2004a, b) to evaluate the rotational deformity of scoliotic vertebrae. Our results confirm that scoliotic spines can be distinguished from non-scoliotic vertebral columns by a combination of different asymmetries of the individual vertebrae that increase towards the apex of the curve, but are absent at the neutral vertebra. These include the distortion of the vertebral body towards the convex side, deviation of the spinous processes, asymmetric pedicular width, facet joints and lateral wedging of the vertebral bodies as well as abnormal sagittal wedging (Smith et al., 1991; Wever et al., 1999).

Our analysis of non-scoliotic vertebral columns showed that these asymmetries, up to a certain degree, often are also a normal feature. Indeed, it is long known that a faint right convex curvature in the mid to lower thoracic region is physiological (Sabatier, 1775; Farkas, 1941; Taylor, 1983). Similarly, Sevastik et al. (1995) and Kouwenhoven et al. (2006) found a slight vertebral rotation to the left of the upper thoracic vertebrae, and to the right of the mid and lower thoracic vertebrae in the majority of normal spines. Others confirmed significant differences in the sagittal orientation and width of the articular facets (Cyron and Hutton,

1980; Singer et al., 1988; Masharawi et al., 2004; 2005), and right convex lateral wedging of the vertebral bodies (Masharawi et al., 2008).

Some of the observed asymmetries in the KNM-WT 15000 spine could therefore be explained by normal asymmetries, whereas others might also be due to measurement errors. This probably includes the observed pedicle thickness asymmetry in the mid-thoracic region. Like previous studies based on a MicroScribe or a similar coordinate measuring machine (Parent et al., 2002; von Cramon-Taubadel et al., 2007; Sholts et al., 2011), we found an average error of measurement of the 3D landmarks of about 0.5 mm. However, individual landmarks can have higher errors of measurement. For example, they are 1.59 mm and 0.67 mm in landmarks 6 and 15, respectively, that are used to calculate the thickness of the right pedicle. Yet, if the right pedicle of T7 had been measured just 0.05 mm thinner, then the ratio of left to right pedicle thickness of T7 would still be within the 3rd to 97th inter-percentile range of normal spines. The fact that this is the only significant asymmetry in the mid-thoracic region strongly suggests that the abnormal difference between left and right pedicle thickness of T7 is due to a measurement error. Moreover, calliper-based measurements of minimal pedicle thickness do not suggest a marked asymmetry at T7 (Haeusler et al., 2011).

Despite some inconsistencies, most asymmetries of KNM-WT 15000 that exceed the 3rd to 97th inter-percentile range of normal spines are associated with other asymmetries that imply a consistent pattern. They suggest a left convex curve at T1 and T2, a possible faint counter curve at T3, and a right convex curve in the lower lumbar region. To get a balanced torso, another left convex counter curve is required. Such a curve can at best be assumed between T4 and T6, although the asymmetries of these vertebrae are still within the normal range of variation.

Thus, the overall curve pattern of KNM-WT 15000 suggests a quadruple curve with the strongest curves being at T1/T2 and L3 to L5, while the two curves in between are at best

very faint. This contrasts to the usual curve patterns of scoliotic spines that mostly present a major mid-thoracic or thoracolumbar/lumbar curve that is accompanied by up to two minor counter curves (Schulthess, 1905; Ponseti and Friedman, 1950; King et al., 1983; Lenke et al., 2001; Qiu et al., 2005). Quadruple curves are extremely rare in scoliotic spines. Therefore, they are not included in the currently most widely used classification systems (King et al., 1983; Lenke et al., 2001; Qiu et al., 2005). Coonrad (1998) described three patients with quadruple curves out of his sample of 2000 scoliotic spines. In these patients, the apices of the four curves were between T4 and T7, at T9, T12, and L3, respectively, or at the intervertebral discs below these vertebrae. This pattern strikingly contrasts to that of KNM-WT 15000, whose proximal curves are more cranial, the distal curve more caudal, and in between is a long, straight section. Moreover, the curves of scoliotic spines usually include at least four to six vertebrae (Ponseti and Friedman, 1950), while they are mostly narrower in KNM-WT 15000.

Individuals with idiopathic scoliosis typically also show an altered sagittal profile of the vertebral column with a flat lower back and hypokyphosis or even lordosis in the thoracic region (Bridwell et al., 1990). Our data and the sagittal wedging angles estimated by Latimer and Ward (1993), however, imply a slightly greater lordosis in the lower lumbar region of KNM-WT 15000 and a compensatorily increased kyphotic wedging at the thoracolumbar transition compared to the modal condition in modern humans. This is consistent with a marked sagittal spinal curvature in KNM-WT 15000, although Been and colleagues (2012) predict a slightly flatter lower back based on the orientation of the inferior articular processes. On the other hand, our data show that sagittal wedging angles of the upper thoracic vertebrae are close to the mean of normal modern humans. This contrasts to the spinous processes of the upper thoracic vertebrae that are decidedly more horizontal compared to those of modern humans (see Fig. 3; Latimer and Ward, 1993). They are thus compatible with hypokyphosis in

the upper thoracic region. However, the recently discovered vertebral column of *Australopithecus sediba* also displays horizontally oriented spinous processes in the upper thoracic vertebrae {Frater, 2013 #11961}. This suggests that the horizontal orientation of the spinous processes is a general characteristic of early hominins rather than pathological.

In conclusion, the observed curves in the coronal plane of the KNM-WT 15000 spine must have another explanation than adolescent idiopathic scoliosis. The long, straight section between the proximal thoracic curves and the distal lumbar curve suggests distinct aetiologies for these curves. Rather than a global spinal deformity, the proximal curves at T1/T2 and T3 might reflect a local dysbalance, perhaps due to growth anomaly or injury.

The asymmetries at the lower lumbar vertebrae of KNM-WT 15000 are mainly restricted to the shape and size of the facet joints of L3 to L5. Walker and Leakey (1993b) describe a post-mortem crushing damage to the left superior articular facet of the Nariokotome boy's last lumbar vertebra A detailed analysis reveals, however, that the tip of the left superior articular facet of L5 is osteophytically remodelled and forms an extra joint with the underside of the left pedicle of L4 (Haeusler et al., 2013). These bony changes must therefore have been acquired *intra vitam* and imply a telescoping subluxation of the left facet joint, most likely due to a traumatic juvenile disc herniation L4–5. The immature age of the Nariokotome boy and the remaining potential for growth likely facilitated bony remodelling of the contiguous articular processes secondary to asymmetrical disc space narrowing. This finding is in good agreement with an analysis of the trabecular microstructure of the pelvis by Volpato et al. (2012). These authors conclude that the right leg of KNM-WT 15000 was more loaded, perhaps due to pain or weakness of the left leg stemming from the disc herniation.

Finally, we find no evidence for the extra-spinal scoliotic bony alterations of KNM-WT 15000 listed by Latimer and Ohman (2001), including asserted rib distortions, clavicular and pelvic asymmetries. Although differences in right and left rib curvatures are evident from

Figs. 7.86 and 7.87 of Walker and Leakey (1993b), they are unsystematic and hence do not indicate a rib hump as suggested by Latimer and Ohman (2001). Importantly, these alleged rib distortions disappear after a minor rearrangement of the ribs. This rearrangement is supported by recently described new rib fragments of KNM-WT 15000, and it makes his thoracic shape completely symmetric (Haeusler et al., 2011). On the other hand, while asymmetry of the three-dimensional shape of the clavicles is frequent in the normal human population (Abdel Fatah et al., 2012), clavicular length differs but by 0.1 mm in KNM-WT 15000 (Walker and Leakey, 1993b). Moreover, the asymmetry at the sternal extremities of the KNM-WT 15000 clavicles can probably be attributed to erosion (Schiess et al., 2006). In addition, the asymmetry of the KNM-WT 15000 sciatic notch, *nota bene* in an individual where ilium and ischium were not yet fused, is not a typical characteristic of idiopathic scoliosis. In fact, in most cases the caudal limit of the spinal curves does not extend to the lumbosacral border (Rigo, 1997). Accordingly, a computed tomography based study found no pelvic asymmetry in patients with adolescent idiopathic scoliosis (Qiu et al., 2012). Rather, the often asymmetric appearance of the hipbones on conventional radiographs was shown to be due to pelvic rotation (Gum et al., 2007).

Summary and Conclusions

Our morphologic and morphometric analysis of the vertebral column of KNM-WT 15000 demonstrates the presence of an anomaly in his upper thoracic region and a second one in the lower lumbar vertebrae. The first anomaly is restricted to vertebrae T1 and T2 and is compatible with a short left convex curve. On the other hand, the lumbar anomaly indicates a right convex curve in vertebrae L3 to L5. The vertebrae between these two regions show no significant deformation in the coronal, sagittal or axial plane. In our principal component analysis of the overall vertebral asymmetry, KNM-WT 15000 therefore groups with normal

individuals. This pattern is at odds with the diagnosis of scoliosis suggested by Latimer and Ohman (2001) and Lovejoy (2005). In fact, scoliosis is not a random accumulation of asymmetries. Patients with juvenile or adolescent idiopathic scoliosis typically have a major mid-thoracic or thoracolumbar / lumbar curve that includes at least five to six vertebrae and is accompanied by one or two adjacent minor counter curves (Schulthess, 1905; Ponseti and Friedman, 1950; King et al., 1983; Lenke et al., 2001; Qiu et al., 2005). There is also no evidence for congenital, neuromuscular or syndromic scoliosis, and the curve pattern of KNM-WT 15000 neither fits with these types of scoliosis. In addition, the recent study by Schiess et al. (2013) refutes the conclusion of Latimer and Ohman (2001) and Ohman et al. (2002) of skeletal dysplasia and thus of syndromic scoliosis in KNM-WT 15000. Furthermore, in contrast to Latimer and Ohman's (2001) assertion, extra-spinal asymmetries in the rib cage are absent in the Nariokotome boy skeleton (Haeusler et al., 2011), and those in the clavicles and hipbones are not characteristic of scoliosis.

The anomalies of the lower lumbar and the uppermost thoracic vertebrae must therefore have different aetiologies as they cannot be attributed to the same pathology. The marked lateral deviation and the osteophytes of the spinous processes of T1 and T2 perhaps resulted from injury or a local growth dysbalance. On the other hand, the asymmetries of the lower lumbar vertebrae are restricted to the articular processes. They imply a collisional subluxation of the left facet joint of vertebrae L4 and L5, most likely as the result of juvenile traumatic disc herniation L4–5 (Haeusler et al., 2013). The asymmetry in length and shape of the adjacent facet joints can be attributed to the juvenile age of the Nariokotome boy and the remaining potential for growth, which allowed for a compensative lengthening of the articular processes to offset the obliquity of the vertebral bodies of L4 and L5.

There is therefore no indication that this important fossil should not be used as a reference for *Homo erectus* skeletal biology, as cautioned by Latimer and Ohman (2001).

Specifically, our results imply that, e.g., stature estimations (Feldesman and Lundy, 1988; Ruff and Walker, 1993; Ruff, 2007) or studies of the lordosis angle (Latimer and Ward, 1993; Been et al., 2012; Williams et al., 2013) are not affected by an allegedly pathological spinal curvature.

Acknowledgements

We thank Emma Mbua and the staff of the National Museums of Kenya, Nairobi, for access to the KNM-WT 15000 fossil and the hospitality during our stay. The study of the extant comparative material was generously permitted by C. van Schaik (Anthropologisches Institut und Museum Zuerich); G. Hotz (Naturhistorisches Museum Basel); S. Ulrich-Bochsler (Historische Anthropologie, Universitaet Bern); T. Uldin, (Anthropologisches Forschungsinstitut Aesch); B. Ruettimann (Medizinhistorisches Institut Zuerich). Financial support was provided by the A.H. Schultz Foundation and the Mäxi Foundation.

Literature

Abdel Fatah, E.E., Shirley, N.R., Mahfouz, M.R., Auerbach, B.M., 2012. A three-dimensional analysis of bilateral directional asymmetry in the human clavicle. Am. J. Phys. Anthropol. 149:547-559.

Asher, M.A., Burton, D.C., 2006. Adolescent idiopathic scoliosis: natural history and long term treatment effects. Scoliosis 1:2.

Been, E., Gómez-Olivencia, A., Kramer, P.A., 2012. Lumbar lordosis of extinct hominins. Am. J. Phys. Anthropol. 147:64-77.

Bookstein, F.L., 1991. Morphometric tools for landmark data geometry and biology. Cambridge University Press, Cambridge.

Bramble, D.M., Lieberman, D.E., 2004. Endurance running and the evolution of *Homo*. Nature 432:345 - 352.

Bridwell, K.H., Betz, R., Capelli, A.M., Huss, G., Harvey, C., 1990. Sagittal plane analysis in idiopathic scoliosis patients treated with Cotrel-Dubousset instrumentation. Spine 15:921-926.

Brown, F., Harris, J., Leakey, R., Walker, A., 1985. Early *Homo erectus* skeleton from west Lake Turkana, Kenya. Nature 316:788-792.

Cheung, K.M., Wang, T., Qiu, G.X., Luk, K.D., 2008. Recent advances in the aetiology of adolescent idiopathic scoliosis. Int. Orthop. 32:729-734.

Cobb, J.R., 1948. Outline for the study of scoliosis. In: Edwards, J.W. (Ed.) Instr. Course Lect. The American Academy od Orthopaedic Surgeons, Ann Arbor, pp 261-275.

Coonrad, R.W., Murrell, G.A., Motley, G., Lytle, E., Hey, L.A., 1998. A logical coronal pattern classification of 2,000 consecutive idiopathic scoliosis cases based on the scoliosis research society-defined apical vertebra. Spine 23:1380-1391.

Cyron, B.M., Hutton, W.C., 1980. Articular tropism and stability of the lumbar spine. Spine 5:168-172.

Dahlberg, G., 1940. Statistical methods for medical and biological students. George Allen & Unwin, London.

Day, M.H., Leakey, R.E.F., 1974. New evidence for the genus *Homo* from East Rudolf, Kenya (III). Am. J. Phys. Anthropol. 41:367-380.

Dean, M.C., Leakey, M.G., Reid, D.J., Schrenk, F., Schwartz, G.T., Stringer, C., Walker, A., 2001. Growth processes in teeth distinguish modern humans from *Homo erectus* and earlier hominins. Nature 414:628-631.

Dimeglio, A., Canavese, F., Charles, P., 2011. Growth and Adolescent Idiopathic Scoliosis: When and How Much? Journal of Pediatric Orthopaedics 31:S28-S36.

Farkas, A., 1941. Physiological scoliosis. J. Bone Joint Surg. Am. 23:607-627.

Feldesman, M.R., Lundy, J.K., 1988. Stature estimates for some African Plio-Pleistocene fossil hominids. J. Hum. Evol. 17:583-596.

Figueiredo, U.M., James, J.I., 1981. Juvenile idiopathic scoliosis. J. Bone Joint Surg. Br. 63-B:61-66.

Goldstein, L.A., Waugh, T.R., 1973. Classification and terminology of scoliosis. Clin Orthop Relat Res 93:10-22.

Graves, R.R., Lupo, A.C., McCarthy, R.C., Wescott, D.J., Cunningham, D.L., 2010. Just how strapping was KNM-WT 15000? J. Hum. Evol. 59:542-554.

Gum, J.L., Asher, M.A., Burton, D.C., Lai, S.M., Lambart, L.M., 2007. Transverse plane pelvic rotation in adolescent idiopathic scoliosis: primary or compensatory? Eur. Spine J. 16:1579-1586.

Haeusler, M., McHenry, H.M., 2004. Body proportions of *Homo habilis* reviewed. J. Hum. Evol. 46:433-465.

Haeusler, M., McHenry, H.M., 2007. Evolutionary reversals of limb proportions in early hominids? Evidence from KNM-ER 3735 (*Homo habilis*). J. Hum. Evol. 53:383-405.

Haeusler, M., Schiess, R., Boeni, T., 2011. New vertebral and rib material point to modern bauplan of the Nariokotome *Homo erectus* skeleton. J. Hum. Evol. 61:575-582.

Haeusler, M., Schiess, R., Boeni, T., 2012. Modern or distinct axial bauplan in early hominins? A reply to Williams (2012). J. Hum. Evol. 63:557-559.

Haeusler, M., Schiess, R., Boeni, T., 2013. Evidence for juvenile disc herniation in a *Homo erectus* boy skeleton. Spine 38:123-128.

Hedequist, D., Emans, J., 2007. Congenital scoliosis: a review and update. J. Pediatr. Orthop. 27:106-116.

James, J.I., 1954. Idiopathic scoliosis; the prognosis, diagnosis, and operative indications related to curve patterns and the age at onset. J. Bone Joint Surg. Br. 36-B:36-49.

Kane, W.J., 1977. Scoliosis prevalence: a call for a statement of terms. Clin Orthop Relat Res:43-46.

King, H.A., Moe, J.H., Bradford, D.S., Winter, R.B., 1983. The selection of fusion levels in thoracic idiopathic scoliosis. J. Bone Joint Surg. Am. 65:1302-1313.

Knapp, T.R., 1992. Technical error of measurement: A methodological critique. Am. J. Phys. Anthropol. 87:235-236.

Kouwenhoven, J.W., Castelein, R.M., 2008. The pathogenesis of adolescent idiopathic scoliosis: review of the literature. Spine 33:2898-2908.

Kouwenhoven, J.W., Vincken, K.L., Bartels, L.W., Castelein, R.M., 2006. Analysis of preexistent vertebral rotation in the normal spine. Spine 31:1467-1472.

Latimer, B., Ohman, J.C., 2001. Axial dysplasia in *Homo erectus*. J. Hum. Evol. 40:A12.

Latimer, B., Ward, C.V., 1993. The thoracic and lumbar vertebrae. In: Walker, A., Leakey, R. (Eds.) The Nariokotome *Homo erectus* Skeleton. Springer, Berlin, pp 266-293.

Lenke, L.G., Betz, R.R., Harms, J., Bridwell, K.H., Clements, D.H., Lowe, T.G., Blanke, K., 2001. Adolescent idiopathic scoliosis: a new classification to determine extent of spinal arthrodesis. J. Bone Joint Surg. Am. 83-A:1169-1181.

Liljenqvist, U.R., Link, T.M., Halm, H.F., 2000. Morphometric analysis of thoracic and lumbar vertebrae in idiopathic scoliosis. Spine 25:1247-1253.

Lordkipanidze, D., Jashashvili, T., Vekua, A., Ponce de Leon, M.S., Zollikofer, C.P., Rightmire, G.P., Pontzer, H., Ferring, R., Oms, O., Tappen, M., Bukhsianidze, M., Agusti, J., Kahlke, R., Kiladze, G., Martinez-Navarro, B., Mouskhelishvili, A.,

Nioradze, M., Rook, L., 2007. Postcranial evidence from early *Homo* from Dmanisi, Georgia. Nature 449:305-310.

Lovejoy, C.O., 2005. The natural history of human gait and posture. Part 1. Spine and pelvis. Gait Posture 21:95-112.

Lowe, T.G., Edgar, M., Margulies, J.Y., Miller, N.H., Raso, V.J., Reinker, K.A., Rivard, C.H., 2000. Etiology of idiopathic scoliosis: current trends in research. J. Bone Joint Surg. Am. 82-A:1157-1168.

MacLarnon, A.M., Hewitt, G.P., 2004. Increased breathing control: Another factor in the evolution of human language. Evolutionary Anthropology 13:181 - 197.

Masharawi, Y., Rothschild, B., Dar, G., Peleg, S., Robinson, D., Been, E., Hershkovitz, I., 2004. Facet orientation in the thoracolumbar spine: three-dimensional anatomic and biomechanical analysis. Spine 29:1755-1763.

Masharawi, Y., Rothschild, B., Salame, K., Dar, G., Peleg, S., Hershkovitz, I., 2005. Facet tropism and interfacet shape in the thoracolumbar vertebrae: characterization and biomechanical interpretation. Spine 30:E281-292.

Masharawi, Y., Salame, K., Mirovsky, Y., Peleg, S., Dar, G., Steinberg, N., Hershkovitz, I., 2008. Vertebral body shape variation in the thoracic and lumbar spine: characterization of its asymmetry and wedging. Clin. Anat. 21:46-54.

McHenry, H.M., 1992. Body size and proportions in early hominids. Am. J. Phys. Anthropol. 87:407-431.

Miller, N.H., 1999. Cause and natural history of adolescent idiopathic scoliosis. Orthop. Clin. North Am. 30:343-352, vii.

Mueller, W.H., Martorell, R., 1988. Reliability and accuracy of measurement. In: Lohman, T.G., Roche, A.F., Martorell, R. (Eds.) Anthropometric Standardization Reference Manual. Human Kinetics Books Champaign, Illionois, pp 83-86.

O'Higgins, P., Jones, N., 2006. Tools for statistical shape analysis. Hull York Medical School. http://www.york.ac.uk/res/fme/resources/software.htm, York.

Ohman, J.C., Wood, C., Wood, B., Crompton, R.H., Günther, M.M., Yu, L., Savage, R., Wang, W., 2002. Stature-at-death of KNM-WT l5000. Hum. Evol. 17:79-94.

Parent, S., Labelle, H., Skalli, W., de Guise, J., 2004a. Thoracic pedicle morphometry in vertebrae from scoliotic spines. Spine 29:239-248.

Parent, S., Labelle, H., Skalli, W., de Guise, J., 2004b. Vertebral wedging characteristic changes in scoliotic spines. Spine 29:E455-462.

Parent, S., Labelle, H., Skalli, W., Latimer, B., de Guise, J., 2002. Morphometric analysis of anatomic scoliotic specimens. Spine 27:2305-2311.

Perdriolle, R., Le Borgne, P., Dansereau, J., de Guise, J., Labelle, H., 2001. Idiopathic scoliosis in three dimensions: a succession of two-dimensional deformities? Spine 26:2719-2726.

Ponseti, I.V., Friedman, B., 1950. Prognosis in idiopathic scoliosis. J. Bone Joint Surg. Am. 32A:381-395.

Qiu, G., Zhang, J., Wang, Y., Xu, H., Zhang, J., Weng, X., Lin, J., Zhao, Y., Shen, J., Yang, X., Luk, K.D., Lu, D., Lu, W.W., 2005. A new operative classification of idiopathic scoliosis: a Peking Union Medical College Method. Spine 30:1419-1426.

Qiu, X.S., Zhang, J.J., Yang, S.W., Lv, F., Wang, Z.W., Chiew, J., Ma, W.W., Qiu, Y., 2012. Anatomical study of the pelvis in patients with adolescent idiopathic scoliosis. J. Anat. 220:173-178.

Raggio, C.L., 2006. Sexual dimorphism in adolescent idiopathic scoliosis. Orthop. Clin. North Am. 37:555-558.

Rigo, M., 1997. Pelvis asymmetry in idiopathic scoliosis. Evidence of whole torsional body deformity? In: Sevastik, J.A., Diab, K.M. (Eds.) Research into Spinal Deformities. IOS Press, Amsterdam.

Robinson, C.M., McMaster, M.J., 1996. Juvenile idiopathic scoliosis. Curve patterns and prognosis in one hundred and nine patients. J. Bone Joint Surg. Am. 78:1140-1148.

Robinson, J.T., 1972. Early Hominid Posture and Locomotion. University of Chicago Press, Chicago.

Ruff, C., 2007. Body size prediction from juvenile skeletal remains. Am. J. Phys. Anthropol. 133:698-716.

Ruff, C.B., Walker, A., 1993. Body size and body shape. In: Walker, A., Leakey, R. (Eds.) The Nariokotome *Homo erectus* skeleton. Springer, Berlin, pp 234-265.

Sabatier, M., 1775. Traité complete d'anatomie, ou description de toutes les parties du corps humain. Didot le Jeune, Paris.

Schiess, R., Haeusler, M., 2013. No skeletal dysplasia in the Nariokotome boy KNM-WT 15000 (*Homo erectus*): a reassessment of congenital pathologies of the vertebral column. Am. J. Phys. Anthropol. 150:365–374.

Schiess, R., Haeusler, M., Langenegger, E., 2006. Wie pathologisch ist die Wirbelsäule des Nariokotome Boys KNM-WT 15'000 (*Homo erectus*)? Bull. Schweiz. Ges. Anthropol. 12:13-22.

Schmorl, G., Junghans, H., 1968. Die gesunde und die kranke Wirbelsäule in Röntgenbild und Klinik, 5th edn. G. Thieme, Stuttgart.

Schulthess, W., 1905. Die Pathologie und Therapie der Rückgratsverkrümmungen. In: Joachimssthal (Ed.) Handbuch der Orthopädischen Chirurgie. Gustav Fischer, Jena.

Sevastik, B., Xiong, B., Sevastik, J., Hedlund, R., Suliman, I., 1995. Vertebral rotation and pedicle length asymmetry in the normal adult spine. Eur. Spine J. 4:95-97.

Sholts, S.B., Flores, L., Walker, P.L., Warmlander, S.K.T.S., 2011. Comparison of Coordinate Measurement Precision of Different Landmark Types on Human Crania Using a 3D Laser Scanner and a 3D Digitiser: Implications for Applications of Digital Morphometrics. International Journal of Osteoarchaeology 21:535-543.

Singer, K.P., Breidahl, P.D., Day, R.E., 1988. Variations in zygapophyseal joint orientation and level of transition at the thoracolumbar junction. Preliminary survey using computed tomography. Surg. Radiol. Anat. 10:291-295.

Smith, B.H., 1993. The physiological age of KNM-WT 15000. In: Walker, A., Leakey, R. (Eds.) The Nariokotome *Homo erectus* skeleton. Springer, Berlin, pp 195-220.

Smith, R.M., Pool, R.D., Butt, W.P., Dickson, R.A., 1991. The transverse plane deformity of structural scoliosis. Spine (Phila Pa 1976) 16:1126-1129.

Smith, S.L., 2004. Skeletal age, dental age, and the maturation of KNM-WT 15000. Am. J. Phys. Anthropol. 125:105-120.

Stokes, I.A., 1994. Three-dimensional terminology of spinal deformity. A report presented to the Scoliosis Research Society by the Scoliosis Research Society Working Group on 3-D terminology of spinal deformity. Spine 19:236-248.

Tardieu, C., 1998. Short adolescence in early hominids: infantile and adolescent growth of the human femur. Am. J. Phys. Anthropol. 107:163-178.

Taylor, J.R., 1983. Scoliosis and growth. Patterns of asymmetry in normal vertebral growth. Acta Orthop. Scand. 54:596-602.

Vialle, R., Thevenin-Lemoine, C., Mary, P., 2013. Neuromuscular scoliosis. Orthopaedics & Traumatology-Surgery & Research 99:S124-S139.

Volpato, V., Bondioli, L., Coppa, A., Macchiarelli, R., 2012. Structural dissymmetry in the iliac cancellous network supports postural/gait-related problems in the KNM-WT 15000

early adolescent from Nariokotome. 2nd Meeting of the European Society for the study of Human Evolution, Bordeaux.

von Cramon-Taubadel, N., Frazier, B.C., Lahr, M.M., 2007. The problem of assessing landmark error in geometric morphometrics: theory, methods, and modifications. Am. J. Phys. Anthropol. 134:24-35.

Walker, A., Leakey, R. (Eds.), 1993a. The Nariokotome *Homo erectus* skeleton. Springer, Berlin.

Walker, A., Leakey, R., 1993b. The postcranial bones. In: Walker, A., Leakey, R. (Eds.) The Nariokotome *Homo erectus* Skeleton. Springer, Berlin, pp 95-160.

Weinstein, S.L., Dolan, L.A., Cheng, J.C., Danielsson, A., Morcuende, J.A., 2008. Adolescent idiopathic scoliosis. Lancet 371:1527-1537.

Weinstein, S.L., Zavala, D.C., Ponseti, I.V., 1981. Idiopathic scoliosis: long-term follow-up and prognosis in untreated patients. J. Bone Joint Surg. Am. 63:702-712.

Wever, D.J., Veldhuizen, A.G., Klein, J.P., Webb, P.J., Nijenbanning, G., Cool, J.C., v Horn, J.R., 1999. A biomechanical analysis of the vertebral and rib deformities in structural scoliosis. Eur. Spine J. 8:252-260.

Williams, S.A., 2012. Modern or distinct axial bauplan in early hominins? Comments on Haeusler et al. (2011). J. Hum. Evol. 63:552-556.

Williams, S.A., Ostrofsky, K.R., Frater, N., Churchill, S.E., Schmid, P., Berger, L.R., 2013. The vertebral column of *Australopithecus sediba*. Science 340.

Zihlman, A., Bolter, D., Boesch, C., 2004. Wild chimpanzee dentition and its implications for assessing life history in immature hominin fossils. Proc. Natl. Acad. Sci. U.S.A. 101:10541-10543.

Tables

Table 1. Variables calculated per vertebra (see caption of Fig. 2 for definition of the 3D landmark points)

Variable	Definition
Lateral deviation of spinous process	Least possible angle between spinous process axis (vector[$P_{14}P_{27}$]) and sagittal plane of the vertebral body (defined by P_{10}, P_{12}, and the midpoint between P_2 and $P_{4)}$
Vertebral body torsion	Least possible angle between line connecting the infero-medial corner of the superior articular facets (vector[$P_{20}P_{24}$]) and sagittal plane of the vertebral body (defined by P_{10}, P_{12}, and the midpoint between P_2 and $P_{4)}$
Lateral wedging	Angle between superior and inferior transverse body diameters (P_1P_3 with P_9P_{11})
Sagittal wedging	Angle between superior and inferior sagittal body diameters (P_2P_4 with $P_{10}P_{12}$)
Pedicle root asymmetry	Distance(P_5P_{13}) / distance(P_6P_{15})
Superior articular facet area asymmetry	Area defined by P_{18}, P_{19}, P_{20} and P_{21} / area defined by P_{22}, P_{23}, P_{24} and P_{25}
Inferior articular facet area asymmetry	Area defined by P_{28}, P_{29}, P_{30} and P_{31} / area defined by P_{32}, P_{33}, P_{34} and P_{35}

Table 2. Error of measurement of the 3D landmarks (mm).

Landmark	Type*	mid-lumbar vertebra	mid-thoracic vertebra
1	II	1.40	0.37
2	II	1.05	0.42
3	II	0.97	0.30
4	II	0.69	0.53
5	III	0.64	0.58
6	III	1.59	0.99
7	II	0.54	0.63
8	II	0.41	0.54
9	II	0.70	0.49
10	II	0.54	0.36
11	II	0.51	0.84
12	II	0.59	0.51
13	II	0.48	0.55
14	II	0.55	0.30
15	II	0.67	0.48
16	II	0.44	0.52
17	II	0.45	0.35
18	III	0.81	0.80
19	III	1.21	0.65
20	III	1.16	0.55
21	III	0.90	1.15
22	III	0.54	0.61

23	III	0.18	0.90
24	III	1.55	0.76
25	III	0.34	0.35
26	III	0.41	0.44
27	II	0.29	0.62
28	III	0.45	0.80
29	III	0.36	0.71
30	III	0.45	0.55
31	III	0.37	0.52
32	III	0.53	0.86
33	III	0.41	0.52
34	III	0.35	0.39
35	III	0.77	0.84
Median		0.54	0.55

* defined according to Bookstein (1991)

Table 3. The technical error of measurement calculated for vertebral variables at a mid-lumbar and a mid-thoracic vertebra, respectively.

Variable	Vertebra	Technical error of measurement
Lateral deviation of spinous process (°)	mid-lumbar	1.28
	mid-thoracic	1.90
Vertebral body torsion (°)	mid-lumbar	3.27
	mid-thoracic	4.57
Lateral wedging angle (°)	mid-lumbar	0.55
	mid-thoracic	1.39
Sagittal wedging angle (°)	mid-lumbar	2.68
	mid-thoracic	1.38
Pedicle root asymmetry	mid-lumbar	0.10
	mid-thoracic	0.04
Superior articular facet area asymmetry	mid-lumbar	0.07
	mid-thoracic	0.11
Inferior articular facet area asymmetry	mid-lumbar	0.02
	mid-thoracic	0.04

Table 4. Serial changes of vertebral variables of KNM-WT 15000 compared to the median, standard deviation, 3rd and 97th percentiles of the normal modern human sample (cf. Fig. 5).

	Lateral deviation of spinous process†					Vertebral body torsion					Lateral wedging angle				
Level	WT 15K	Modern humans				WT 15K	Modern humans				WT 15K	Modern humans			
		Median	SD	3rd P	97th P		Median	SD	3rd P	97th P		Median	SD	3rd P	97th P
T1	16.5*	0.0	8.5	-12.5	13.2	96.2	89.7	9.7	82.1	108.6	2.9	-2.7**	5.2	-9.1	5.0
T2	4.4	-0.1	7.1	-11.0	9.8	89.7	89.8	6.4	79.7	95.9	-4.9	-1.9	4.5	-7.2	7.1
T3	1.1	-1.1	6.6	-11.4	9.9	91.3	86.9	4.1	80.3	93.0	-5.4	-1.7	5.9	-8.5	12.0
T4	4.3	0.3	4.4	-6.3	7.0	92.0	89.0	5.6	81.9	99.8	5.7	2.9**	4.7	-4.6	10.5
T5	-	0.6	5.9	-8.6	9.6	-	89.5	9.1	78.9	103.5	-	-0.1	6.4	-8.8	13.3
T6	7.8	-0.2	5.6	-9.2	10.0	90.4	88.0	5.6	76.5	97.6	6.3	-2.4	5.8	-10.5	8.3
T7	0.5	-0.6	7.2	-11.5	10.7	90.0	85.4**	5.3	76.3	92.7	-1.2	3.1**	5.4	-8.1	10.3
T8	-	-2.6	7.5	-12.3	11.7	-	85.1**	8.6	77.5	108.1	-	1.4	5.7	-7.2	11.0
T9	-	-3.2	8.8	-13.4	13.4	-	83.1**	7.9	72.5	98.4	-	2.3	5.8	-10.1	9.5
T10	-	-6.6**	7.6	-15.0	7.0	-	84.1**	7.5	72.2	97.7	-	-2.2**	4.5	-7.6	5.7
T11	-7.7	-6.2**	8.1	-14.4	9.7	84.4	84.3**	8.5	71.5	98.1	-3.6	-1.3	3.9	-6.6	4.5

T12	-	-5.4**	8.9	-18.7	11.3	-	84.4**	8.4	75.2	99.3	-	-1.8	5.2	-7.8	8.7
L1	-	-1.9	8.2	-15.6	10.9	-	88.7	5.2	80.7	97.7	-7.1	-2.6**	5.6	-8.9	10.4
L2	-	-1.4	6.7	-11.7	9.0	-	86.2**	6.4	79.4	99.3	-	-1.8	6.8	-5.6	9.1
L3	6.1	-2.0	6.3	-12.7	8.8	97.7	87.2**	4.5	82.1	95.8	-2.9	1.4	7.3	-6.6	5.8
L4	6.1	-0.9	6.0	-10.1	8.8	89.2	86.6	9.6	82.2	113.6	-1.8	-1.7**	3.6	-5.5	6.4
L5	1.7	-1.5	4.9	-10.8	5.4	87.1	87.1	7.1	69.5	91.5	-5.7	-2.5**	3.9	-8.9	5.2

	Sagittal wedging angle					Superior articular facet area asymmetry					Inferior articular facet area asymmetry				
Level	WT 15K	Modern humans				WT 15K	Modern humans				WT 15K	Modern humans			
		Median	SD	3rd P	97th P		Median	SD	3rd P	97th P		Median	SD	3rd P	97th P
T1	-5.3	-5.3**	7.5	-15.5	8.1	1.14	0.97	0.19	0.83	1.32	0.72*	0.92	0.15	0.74	1.24
T2	-2.0	-4.6**	8.1	-16.6	8.5	1.22	1.00	0.14	0.79	1.28	1.08	0.93**	0.11	0.80	1.19
T3	-4.4	-3.2	7.5	-13.2	10.0	1.08	1.00	0.15	0.79	1.31	1.18	0.92**	0.16	0.63	1.20
T4	-2.1	-3.5**	4.7	-10.4	4.6	1.04	1.07	0.16	0.78	1.31	0.94	0.96	0.30	0.64	1.22
T5	-	-5.4**	6.3	-10.2	9.3	-	0.98	0.20	0.66	1.38	-	0.93	0.16	0.64	1.20
T6	-5.0	-6.3**	5.6	-14.2	6.7	0.98	0.98	0.14	0.78	1.26	0.60	0.95	0.21	0.58	1.28
T7	-6.1	-5.5**	6.0	-17.1	3.9	1.03	1.05	0.25	0.72	1.33	0.72	0.94	0.33	0.68	1.34

T8	-	-6.7**	6.0	-17.2	3.3	-	1.06	0.18	0.83	1.37	-	1.01	0.17	0.74	1.31
T9	-	-5.0**	8.2	-14.5	9.8	-	1.02	0.13	0.77	1.22	-	1.00	0.16	0.82	1.31
T10	-	-3.7**	5.0	-8.7	7.6	0.84	1.02	0.17	0.71	1.30	0.92	0.89**	0.15	0.78	1.19
T11	-7.9	-5.5**	5.7	-10.8	7.9	1.06	1.04	0.15	0.81	1.25	1.21	0.95	0.31	0.74	1.40
T12	-	-5.8**	7.4	-13.1	10.1	-	1.01	0.16	0.84	1.34	-	0.98	0.15	0.80	1.28
L1	-8.4	-4.2**	5.4	-10.0	8.2	-	1.00	0.16	0.69	1.25	-	1.01	0.20	0.88	1.30
L2	-	-1.1	5.5	-7.7	8.9	1.06	1.01	0.16	0.82	1.31	0.93	1.02	0.14	0.88	1.36
L3	8.9	1.5	6.2	-8.4	10.7	0.81	0.98	0.15	0.69	1.19	1.30	1.04	0.24	0.90	1.42
L4	9.5	4.8**	5.6	-4.7	13.9	0.93	0.99	0.21	0.79	1.25	1.04	1.07**	0.14	0.88	1.30
L5	14.7	9.0**	9.9	-10.4	20.9	1.26*	0.98	0.10	0.90	1.25	1.08	1.11**	0.18	0.77	1.31

Pedicle root asymmetry

Level	WT 15K	Modern humans			
		Median	SD	3rd P	97th P
T1	0.80	0.93	0.38	0.67	1.36
T2	0.70*	0.98	0.14	0.76	1.18
T3	0.93	0.95	0.15	0.84	1.32

T4	0.76	0.91**	0.14	0.74	1.11
T5	-	0.94	0.14	0.67	1.18
T6	0.78	0.97	0.27	0.61	1.39
T7	0.72*	1.02	0.18	0.73	1.34
T8	-	0.96	0.19	0.63	1.40
T9	-	1.03	0.23	0.81	1.33
T10	-	1.01	0.14	0.78	1.18
T11	0.87	0.98	0.14	0.77	1.19
T12	-	0.98	0.13	0.80	1.19
L1	-	1.00	0.11	0.87	1.24
L2	-	0.99	0.12	0.74	1.18
L3	1.11	0.99	0.12	0.80	1.22
L4	0.98	1.01	0.12	0.90	1.27
L5	1.01	1.01	0.08	0.88	1.19

[†] Negative angles of lateral deviation of the spinous process denote a deviation to the right. Vertebral body torsion below 90° denotes torsion to the left. Negative lateral wedging angles denote wedging to the left. Negative sagittal wedging angles denote kyphotic wedging. Ratios below 1.0 signify that the dimension on the right side is larger.

* Data points of KNM-WT 15000 outside the 3rd-97th inter-percentile range of modern humans.

** Statistically significant different from perfect symmetry ($P < 0.05$, one-sample t-test)

Table 5. Principal Component Analysis loadings (correlation matrix) on the roots of the means of the squared deviations from perfect symmetry for eigenvalues greater than 1.

	PC1	PC2
Eigenvalue	2.869	1.689
Variance explained (%)	40.99	24.14
Variance explained (cumulative %)	40.99	65.13
Sagittal wedging	0.788	-0.353
Lateral wedging	0.840	-0.046
Pedicle root asymmetry	0.825	-0.441
Superior facet area asymmetry	0.383	0.742
Lateral deviation of spinous process	0.359	0.401
Inferior facet area asymmetry	0.422	0.800
Vertebral body torsion	0.639	-0.132

Figure captions

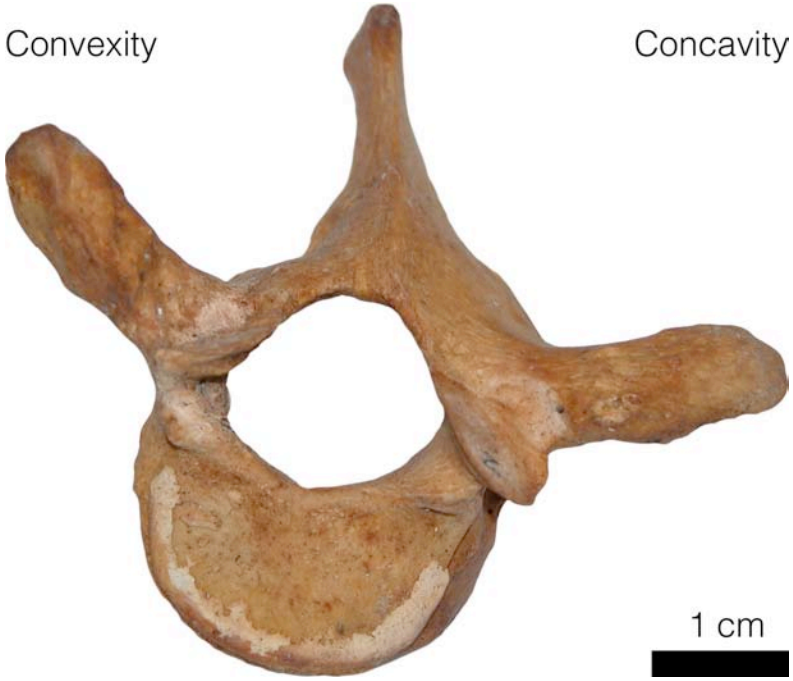

Figure 1. Modern human thoracic vertebra (superior view) showing the torsional deformity of scoliosis with distortion of the vertebral body towards the convex side of the curve, whereas the spinous process is pointed to posterior and then bends to the convex side. Also pedicular width, lamina thickness, and facet joints are asymmetric, and the transverse process deviates to posterior at the convex side of the curve, which is associated with a rib hump on the convexity of the scoliotic curve.

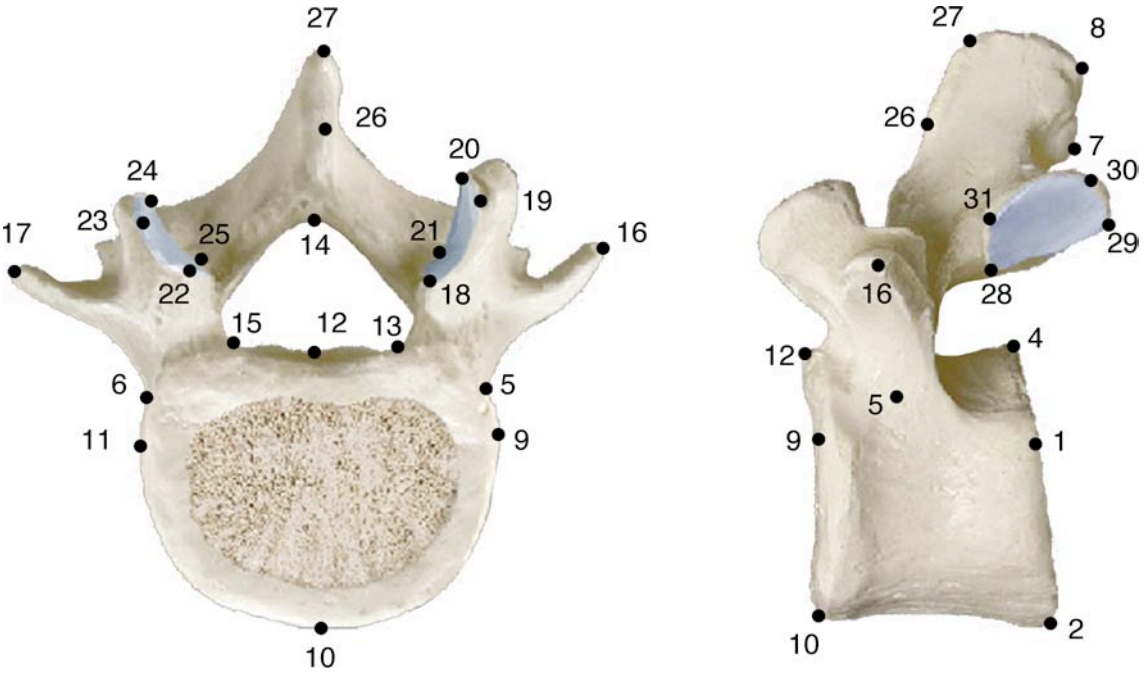

Figure 2. The 35 three-dimensional landmark points measured per vertebra. Inferior vertebral body surface: (P_1, P_3) lateralmost points, (P_2, P_4) most anterior/posterior points on mid-sagittal plane, (P_5, P_6) basis of pedicle on the pedicle axis in lateral view. Spinous process: (P_7) corner between lamina and inferior side of the spinous process in the mid-sagittal plane, (P_8) dorso-inferior extremity. Superior vertebral body surface: (P_9, P_{11}) lateralmost points, (P_{10}, P_{12}) most anterior/posterior points on mid-sagittal plane, (P_{11}) lateralmost points. Vertebral canal: (P_13, P_{15}) basis of pedicle, (P_{14}) most postero-superior point. (P_{16}, P_{17}) Lateral extremity of costal process, respectively transverse process. Superior articular facet: (P_{18}, P_{22}) supero-medial extremity, (P_{19}, P_{23}) supero-lateral extremity, (P_{20}, P_{24}) infero-lateral extremity, (P_{21}, P_{25}) infero-medial extremity. Spinous process: (P_{26}), midpoint superior, (P_{27}) postero-superior extremity. Inferior articular facet: (P_{28}, P_{32}) supero-medial extremity, (P_{29}, P_{33}) infero-medial extremity, (P_{30}, P_{34}) infero-lateral extremity, (P_{31}, P_{35}) supero-lateral extremity.

Figure 3: Superior view (top) and lateral view (bottom) of the praesacral vertebrae of KNM-WT 15000 including the new fragments described in Haeusler et al. (2011). Vertebrae identification is according to Haeusler et al. (2011). Note the lateral deviation of the spinous process of T1 and the unilateral osteophyte on the spinous process of T2 (arrows). Vertebrae

T5 and T8 are missing. Missing parts reconstructed from mirror images are semi-transparent. Scale bars equal 5 cm. A colour version of the Figure is available online.

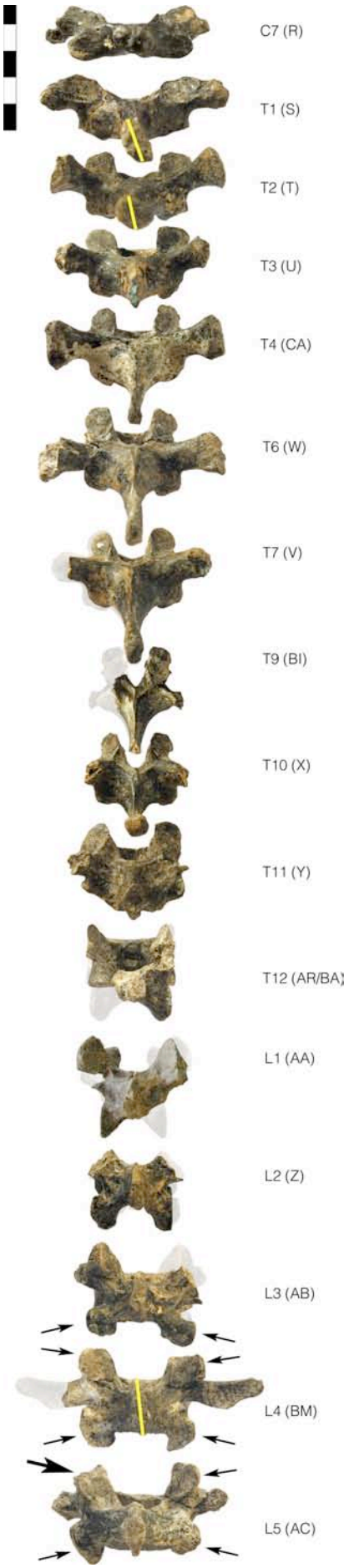
C7 (R)
T1 (S)
T2 (T)
T3 (U)
T4 (CA)
T6 (W)
T7 (V)
T9 (BI)
T10 (X)
T11 (Y)
T12 (AR/BA)
L1 (AA)
L2 (Z)
L3 (AB)
L4 (BM)
L5 (AC)

Figure 4: Dorsal view of the praesacral vertebrae of KNM-WT 15000 including the new fragments described in Haeusler et al. (2011). Vertebrae identification is according to Haeusler et al. (2011). Note the oblique orientation of the tips of the spinous processes of T1, T2 and L4 (highlighted by yellow lines) and the asymmetric facet joints L3–4, L4–5 and L5–S1 (arrows). The left superior articular process of L5 is osteophytically remodelled (thick arrow). Missing parts reconstructed from mirror images are semi-transparent. Scale bar equals 5 cm. A colour version of the Figure is available online.

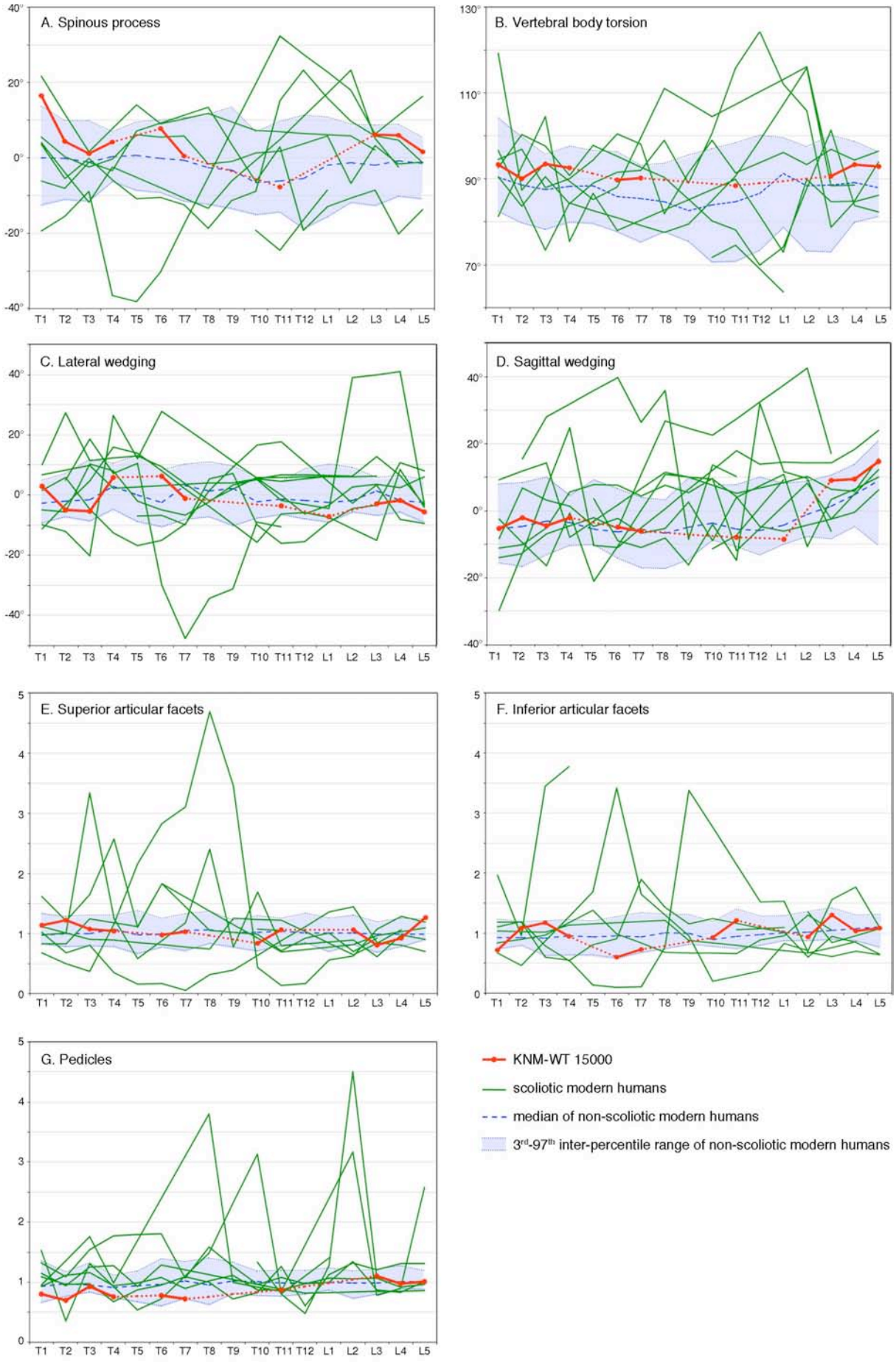
A. Spinous process
B. Vertebral body torsion
C. Lateral wedging
D. Sagittal wedging
E. Superior articular facets
F. Inferior articular facets
G. Pedicles
T1 T2 T3 T4 T5 T6 T7 T8 T9 T10 T11 T12 L1 L2 L3 L4 L5
KNM-WT 15000
scoliotic modern humans
median of non-scoliotic modern humans
3rd-97th inter-percentile range of non-scoliotic modern humans

Figure 5: Serial changes along the thoracolumbar spinal column of KNM-WT 15000, non-scoliotic modern humans and scoliotic modern humans for A, the angle between the axis of the spinous process and the sagittal plane of the vertebral body, B, the angle between the line connecting the superior articular facets and the sagittal plane of the vertebral body, C, the angle between superior and inferior transverse body diameters, D, the angle between superior and inferior sagittal vertebral body diameters, E, the ratio of left to right superior articular facet areas, F, the ratio of left to right inferior articular facet areas, and G, the ratio of left to right pedicle root thickness. A colour version of the Figure is available online.

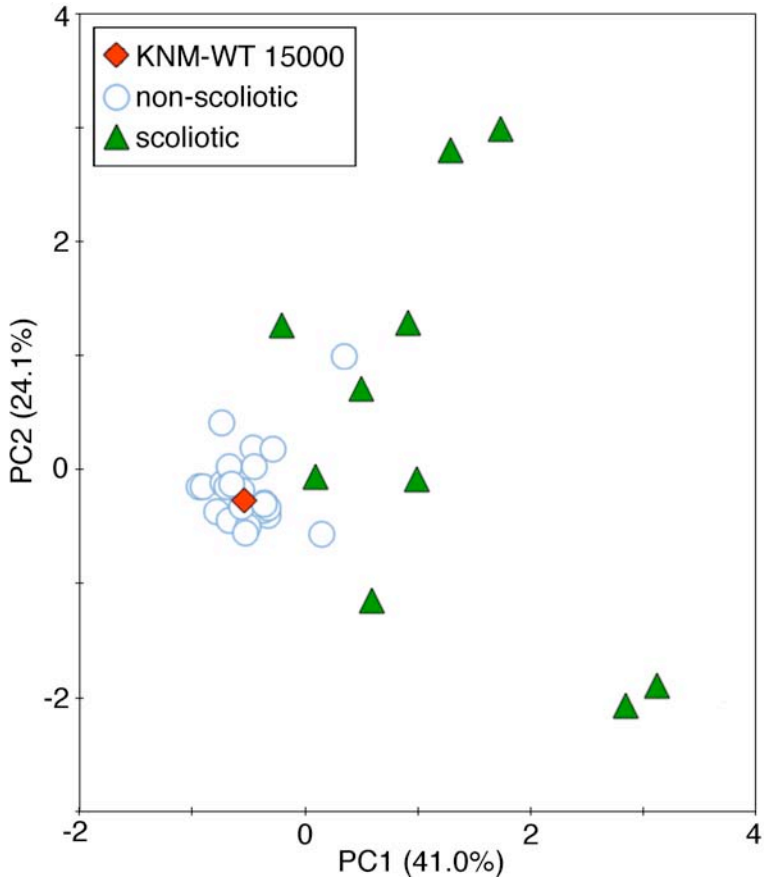

Figure 6. Principal component analysis of vertebral variables for non-scoliotic and scoliotic spines. KNM-WT 15000 groups with non-scoliotic spines. A colour version of the Figure is available online.